Palaeoenvironmental reconstruction and biostratinomic analysis of the Jurassic Yanliao Lagerstätte in northeastern China

Zixiao Yang[a], Shengyu Wang[a], Qingyi Tian[a], Bo Wang[b], Manja Hethke[c], Maria E. McNamara[d], Michael J. Benton[e], Xing Xu[f], Baoyu Jiang[a,*]

[a] *Center for Research and Education on Biological Evolution and Environments, School of Earth Sciences and Engineering, Nanjing University, Nanjing 210023, China*

[b] *Nanjing Institute of Geology and Palaeontology, Chinese Academy of Sciences, Nanjing 210008, China*

[c] *Institut für Geologische Wissenschaften, Fachbereich Geowissenschaften, Freie Universität Berlin, Malteserstrasse 74–100, D–12249 Berlin, Germany*

[d] *School of Biological, Earth and Environmental Sciences, University College Cork, Distillery Fields, North Mall, Cork T23 TK30, Ireland.*

[e] *School of Earth Sciences, University of Bristol, Bristol BS8 1RJ, UK.*

[f] *Key Laboratory of Vertebrate Evolution and Human Origins, Institute of Vertebrate Paleontology and Paleoanthropology, Chinese Academy of Sciences, Beijing 100044, China*

[*] *Corresponding author. Email: byjiang@nju.edu.cn*

Abstract

The Middle–Upper Jurassic Yanliao Lagerstätte contains numerous exceptionally preserved fossils of aquatic and land organisms, including insects, salamanders, dinosaurs, pterosaurs and mammaliaforms. Despite extensive study of the diversity and evolutionary implications

of the biota, the palaeoenvironmental setting and taphonomy of the fossils remain poorly understood. We reconstruct both the palaeoenvironment of the Daohugou area (one of the most famous Yanliao fossil areas), and the biostratinomy of the fossils. We use high-resolution stratigraphic data from field investigation and excavations to document in detail the stratigraphic succession, lithofacies, facies associations, and biostratinomic features of the Lagerstätte. Our results show that frequent volcanic eruptions generated an extensive volcaniclastic apron and lake(s) in the studied area. The frequent alternation of thin lacustrine deposits and thick volcaniclastic apron deposits indicates either that the studied area was located in the marginal regions of a single lake, where the frequent influx of volcaniclastic apron material caused substantial fluctuations in lake area and thus the frequent lateral alternation of the two facies, or that many short-lived lakes developed on the volcaniclastic apron. Most terrestrial insects were preserved in the laminated, normally graded siltstone, claystone and tuff facies that form many thin intervals with deposits of graded sandstone, siltstone and tuff in between. Within each interval the terrestrial insects occur in many laminae associated with abundant aquatic organisms, but are particularly abundant in some laminae that directly underlie tuff of fallout origin. Most of these terrestrial insects are interpreted to have been killed in the area adjacent to the studied palaeolake(s) during volcanic eruptions. Their carcasses were transported by influxes of fresh volcaniclastic material, primarily meteoric runoff and possibly minor distal pyroclastic flow into the palaeolake(s), and were buried in palaeolake deposits prior to extended decay probably due to a combination of rapid vertical settling, ash fall and water turbulence.

Keywords: Palaeolake; Volcanism; Taphonomy; Ecosystem; Middle–Late Jurassic; Yanliao Biota

1 Introduction

The Middle to Upper Jurassic lacustrine deposits in the region encompassing the confluence of Inner Mongolia, Hebei and Liaoning, northeastern China, preserve numerous exceptionally preserved fossils of land and aquatic organisms (Fig. 1), including plants (algae, mosses, lycophytes, sphenophytes, ferns, seed ferns, cycadophytes, ginkgophytes and conifers), invertebrates (bivalves, anostracans, spinicaudatans, arachnids and insects) and vertebrates (fish, salamanders, squamates, pterosaurs, dinosaurs and mammaliaforms) (Huang et al., 2006; Sullivan et al., 2014; Pott and Jiang, 2017). Many of these taxa represent the earliest examples of their respective clades or shed light on key evolutionary transitions (e.g. Gao and Shubin, 2003; Ji et al., 2006; Luo et al., 2007; Xu et al., 2009; Lü et al., 2010; Luo et al., 2011; Xu et al., 2011; Huang et al., 2012; Bi et al., 2014; Cai et al., 2014; Xu et al., 2015). These fossils were originally considered to be members of the Early Cretaceous Jehol Biota (Wang, 2000; Wang et al., 2000), but subsequently proved to be of Middle–Late Jurassic age; they are currently referred to as the Daohugou Biota (e.g. Zhang, 2002) or as part of the Yanliao Biota (e.g. Ren et al., 2002; Zhou et al., 2010; Xu et al., 2016). This paper uses the latter term, as the extent to which the term “Daohugou Biota” is applicable to strata containing similar fossils outside the Daohugou area is currently debated (Zhou et al., 2010; Huang, 2016; Xu et al., 2016). The Yanliao Biota spans about 10 million years and is divided into two phases: the Bathonian–Callovian Daohugou phase and the Oxfordian Linglongta phase, named after representative fossil localities (Xu et al., 2016).

Fossils of the Yanliao Biota are often well articulated and exceptionally preserved. Available evidence indicates that many are autochthonous or parautochthonous, or

allochthonous with very limited evidence of decay. Examples include (i) densely packed valves of clam shrimps (Spinicaudata) that preserve delicate carapace ornamentation and sometimes remains of soft tissue such as the head, telson, antennae and eggs (Shen et al., 2003; Liao et al., 2017); (ii) Ginkgoales with leaves attached to shoots and with ovule clusters connected to the peduncle (Zhou et al., 2007); (iii) cicadas exhibiting fragile structures such as filiform antennae, tarsomeres with spines and hairs, and abdominal appendages (Wang et al., 2013); (iv) salamanders with various soft-tissue features such as body outlines, gill rakers, external gill filaments, caudal fins, eyes, livers, and even intestinal contents (Gao et al., 2013); (v) pterosaurs preserving exquisite integumentary structures including keratinous ungual sheaths, multi-layered wing membrane structures and densely packed melanosomes (Kellner et al., 2010; Li et al., 2014); (vi) dinosaurs with preservation of filamentous, ribbon-like and pennaceous feathers (and their constituent melanosomes) (Xu and Zhang, 2005; F. Zhang et al., 2008; Xu et al., 2009; Xu et al., 2011; Li et al., 2014); and (vii) mammaliaforms with preserved hair, patagia and skin (Bi et al., 2014; Ji et al., 2006; Luo et al., 2007; Meng et al., 2006). These fossils have contributed significantly to our understanding of Jurassic terrestrial ecosystems, especially in terms of the evolution of integumentary structures in paravian dinosaurs and mammaliaforms (feather and fur, respectively), and the ecological diversification of mammaliaforms (Xu et al., 2014; Martin et al., 2015). The biota is rapidly emerging as one of the most important Mesozoic Lagerstätten.

Despite extensive research on the biotic diversity and evolutionary significance of the Yanliao Biota, the palaeoenvironmental setting is poorly understood (Wang et al., 2009; Liu et al., 2010; Wang et al., 2013; Na et al., 2015; Huang, 2016; Xu et al., 2016). It is widely

accepted that the fossils are hosted within laminated lacustrine deposits. It is unclear, however, whether these deposits represent a single lake or several lakes. The terrestrial members of the biota are considered to have been killed predominantly by volcanic activity based on the extensive distribution of volcanic rocks in the Yanliao sequences (e.g. Liu et al., 2010; Wang et al., 2010; Wang et al., 2013), but the biostratinomy of the fossils is poorly understood.

In this paper, we present the results of a systematic study of the sedimentology and palaeoenvironment of the Middle–Upper Jurassic sequence in the Daohugou area (Fig. 1). Our results shed light on key issues such as the origin of the palaeolakes, the mode of sedimentological deposition and the nature of the surrounding ecosystem, in addition to environmental factors that potentially influenced the exceptional fossil preservation that is characteristic of the biota.

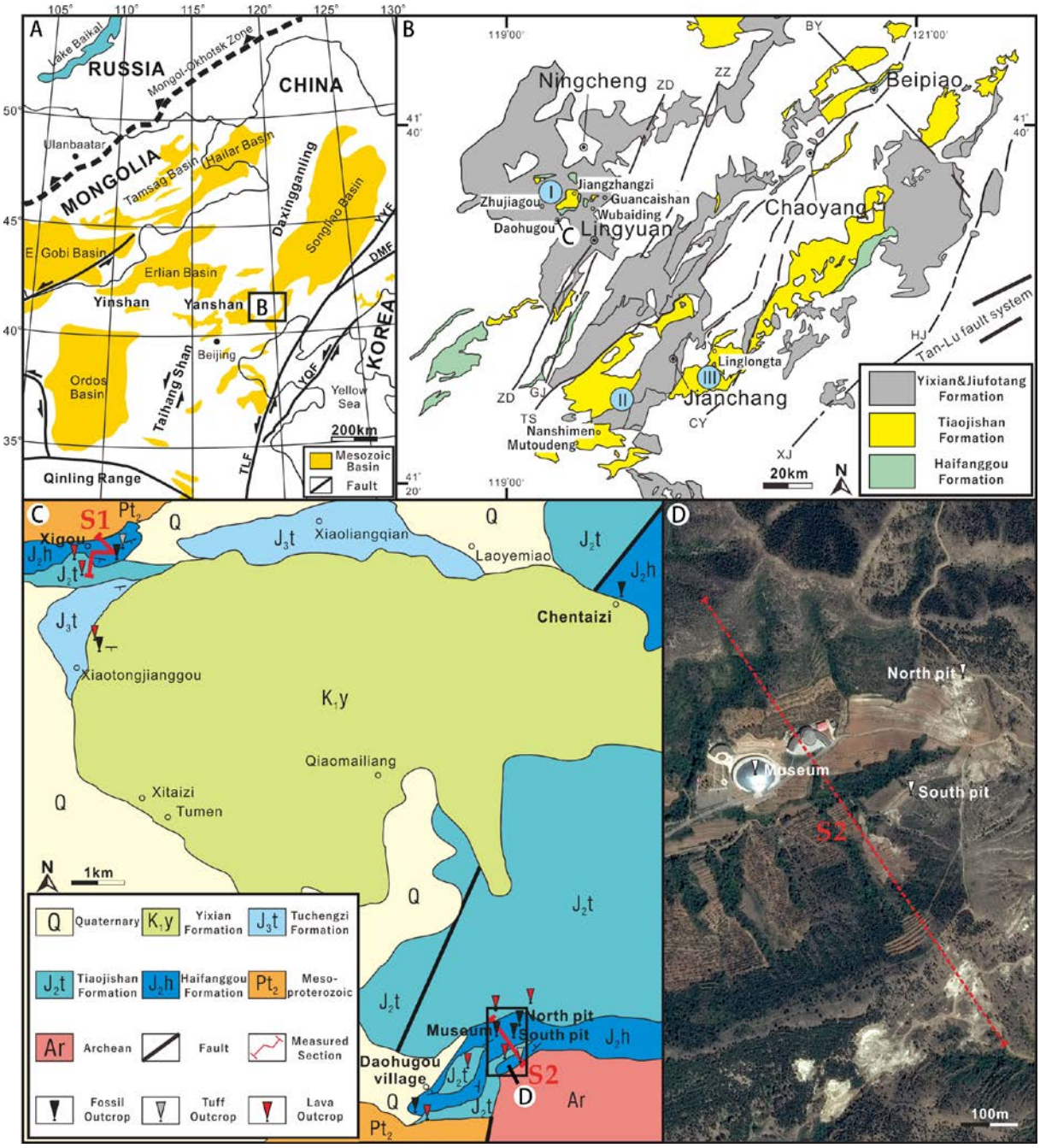

Fig. 1 Geological and geographic setting of the studied area. A. Tectonic framework and distribution of the Mesozoic basins in the Yinshan–Yanshan tectonic belt (modified from Meng, 2003 and Y. Zhang et al., 2008); DMF, Dunhua–Mishan fault; TLF, Tan–Lu fault YYF; YQF, Yalvjiang–Qingdao fault; Yilan–Yitong fault. B. Distribution of the Yixian/Jiufotang, Tiaojishan, and Haifanggou formations in a series of northeast-oriented basins (modified from Jiang and Sha, 2006); I, Lingyuan–Sanshijiazi basin; II, Jianchang basin; III, Jinlingsi–

Yangshan basin; BY, Beipiao–Yixian fault; CY, Chaoyang–Yaowangmiao fault; GJ, Western Guojiadian Basin fault; HJ, Hartao–Jinzhou fault; TS, Western Tangshenmiao Basin fault; XJ, Xipingpo–Jinxi fault; ZD, Zhangjiayingzi–Daoerdeng fault; ZZ, Zhuluke–Zhongsanjia fault. C–D. Geological sketch map (C) and Google Earth satellite image (D) showing the studied outcrops and sections (modified from Liu et al., 2004).

2 Geological setting

The studied area lies at the easternmost edge of the Yinshan–Yanshan tectonic belt (Davis et al., 1998; Y. Zhang et al., 2008), which extends westward at least 1100 km from China's east coast to Inner Mongolia along the northern edge of the North China craton (Fig. 1A). This belt is interpreted as having formed under the far-field effects of synchronous convergence of two plates (the Siberian in the north and the palaeo-Pacific in the east) toward the East Asian continent, during the Middle Jurassic to Early Cretaceous (Nie et al., 1990; Yin and Nie, 1996; Ziegler et al., 1996; Y. Zhang et al., 2008). Structures in the western and central parts of the belt trend predominantly eastward, whereas those in the easternmost part trend predominantly northeastward. The most obvious fold structures are synclines (and synforms) filled with Jurassic and Cretaceous strata; these are separated from anticlines with Precambrian rocks at the core by thrust and reverse faults that dip away from syncline hinges (Davis et al., 1998).

The Yanliao Biota was discovered in the Jurassic Haifanggou and Tiaojishan formations (or Lanqi Formation in studies earlier than the 1990s) in three of these northeast-trending synclines (and synforms), belonging to the following basins: Lingyuan-Sanshijiazi (localities

in the Daohugou, Zhujiagou and Jiangzhangzi areas in southeastern Inner Mongolia, and the Wubaiding and Guancaishan areas in Western Liaoning Province); Jianchang (localities in the Mutoudeng and Nanshimen areas in northern Hebei Province); and Jinlingsi-Yangshan (the Daxishan locality in Linglongta Town, Western Liaoning Province) (Fig. 1B) (Wang et al., 1989; Wang et al., 2005; Sullivan et al., 2014; Huang, 2016; Xu et al., 2016). The Daohugou area in this paper includes the fossil localities at Xigou, Chentaizi and Daohugou villages (Fig. 1C).

The Jurassic strata in these basins unconformably overlie Triassic (or older) strata, and unconformably underlie the Lower Cretaceous Yixian and Jiufotang formations that yield the Jehol Biota (Figs. 1B–C and 2A). The Jurassic sequence consists of two stratigraphic successions bounded by a regional unconformity. The lower succession comprises the volcanic Xinglonggou Formation and the overlying coal-bearing Beipiao Formation. The upper succession is composed of the volcanic Haifanggou and Tiaojishan formations and the overlying Tuchengzi Formation (Wang et al., 1989). The geochronological framework of the sequence is constrained by radiometric dating, which indicates that the Xinglonggou, Tiaojishan and Tuchengzi formations have ages of 177 Ma, 166–153 Ma and 154–137 Ma, respectively (Yang and Li, 2008; Xu et al., 2012; Xu et al., 2016).

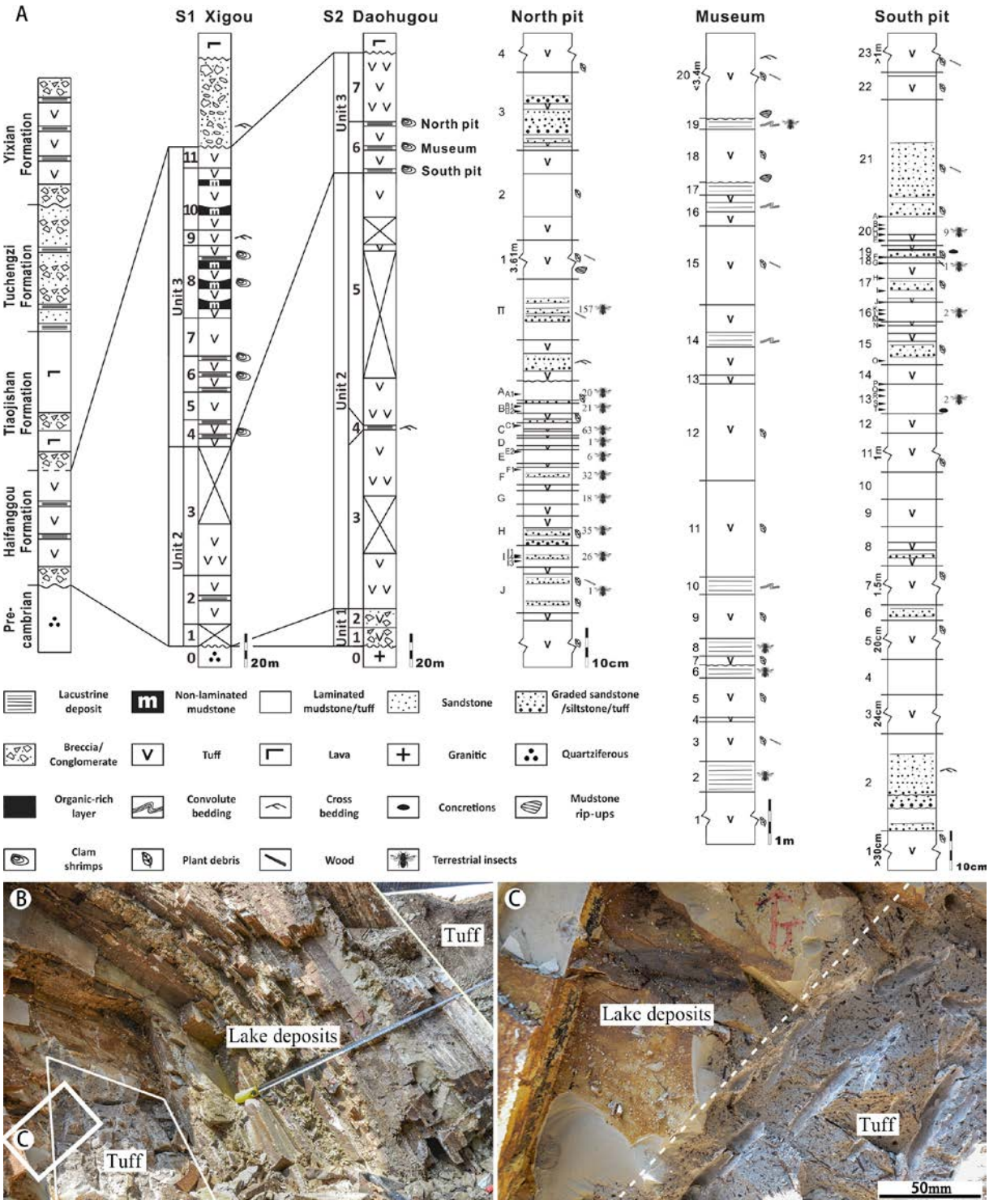

Fig. 2 A. Stratigraphy (left) of the Mesozoic in general and the Haifanggou Formation in particular (S1, S2, locations shown in Fig. 1C) in the Daohugou area, and high-resolution sections (right) from two excavation pits and the Daohugou Palaeontological Fossil Museum (locations shown in Fig. 1C–D) showing numbers and occurrence horizons of collected

157 terrestrial insects. B. Excavated section in North pit shows that lacustrine deposits directly
158 overlie and underlie crudely bedded tuffs (bottom is on the lower left). C. Close-up view of
159 the transition from crudely bedded tuff to laminated lake deposits.

160 The strata that contain the Yanliao Biota in the Daohugou area, the Daohugou Beds, were
161 assigned to the Haifanggou Formation (Wang et al., 1989; Zhang, 2002; Shen et al., 2003;
162 Huang et al., 2006; Jiang, 2006), which was considered to be coeval with the Jiulongshan
163 Formation in Beijing and Hebei (Ren et al., 2002; Shen et al., 2003; Huang et al., 2006; Jiang,
164 2006). In the studied area, the Haifanggou Formation unconformably overlies Archean granite
165 gneiss or Mesoproterozoic quartz sandstone and conglomerate, and conformably or locally
166 unconformably underlies volcanic breccia, tuffaceous conglomerate and intermediate or basic
167 lava of the Tiaojishan Formation (Figs. 1C and 2A). It is worth noting that the local low-angle
168 unconformity between the Haifanggou and Tiaojishan formations (Huang, 2015) is an
169 example of a volcanic unconformity rather than an unconformity in conventional stratigraphy
170 that represents a significant hiatus or gap in the stratigraphic succession. Volcanic
171 unconformities can be generated during the construction of a central volcanic edifice or a
172 stratovolcano involving destructive processes such as major sector failures or collapse
173 calderas, or in successive eruptions (i.e. inter-eruptions) that are separated by short periods of
174 repose, or even between different pulses of the same eruption (intra-eruption), as volcanic
175 deposits are strongly topographically dependent and may have great erosive capacity when
176 they pass over poorly consolidated pyroclastic or sedimentary materials, as is obvious in the
177 case of lava flows and most pyroclastic density current deposits and lahars. Thus, significant
178 minor unconformities may exist in the interior of a single eruptive unit or in the basal or upper

contact zones of volcanic units (Martí et al., 2018), and yet these need not indicate the passage of appreciable amounts of time.

Recently determined radiometric ages for the volcanic rocks overlying the fossil-bearing strata in the Daohugou area include 165–164 Ma (Chen et al., 2004), 159.8 Ma (He et al., 2004) and 164–158 Ma (Liu et al., 2006). These values indicate a largely Bathonian to Callovian age for the Haifanggou Formation, corresponding to the older Daohugou phase of the Yanliao Biota (Xu et al., 2016).

3 Methods

Two relatively continuous sections were measured (S1 and S2 in Figs. 1C and 2A). Small-scale pits (about 15–20 m^2 in area and 3–4 m deep; North pit and South pit in Figs. 1C–D and 2) were excavated into two fossiliferous parts of section S2 to document, at a sub-centimetre scale, the diversity, abundance, completeness and articulation, and plan-view orientation (Supplementary material Appendix 1) of the fossils and the lithology of the host strata. Freshly exposed rock was hard to split layer by layer, so we tried frost-splitting particularly for tough large rock slabs, which were frozen in refrigerating cabinets for over 24h and then exposed to sunshine until they were ready for splitting. Slab thicknesses were determined by splitting readiness, ranging from 20 mm to 155 mm. The slabs of each interval were then searched for fossils layer by layer. The intervals that were fossiliferous and quantitatively studied were named alphabetically in a stratigraphically descending order, except for interval Π, which was highest in the North pit but was discovered later than some of the lower intervals. A detailed quantitative palaeobiological analysis of the fossils will be

presented elsewhere (Wang et al., in prep.). Stratigraphically between the two excavated parts, an additional fossiliferous part of section S2 exposed in the Daohugou Palaeontological Fossil Museum (Figs. 1C–D and 2) was measured for lithology and fossil content. A total of 216 thin sections of representative lithofacies were prepared for petrographic analysis.

4 Results

4.1 Stratigraphy

The two measured sections (S1 and S2 in Fig. 2A) reveal that the Daohugou Beds in the Daohugou area consist of three units, in ascending order: (1) greenish grey, massive lapilli tuff-breccia with rare grey, laminated mudstone intercalations; (2) greenish to pinkish grey, crudely bedded to massive tuff with rare intercalations of grey, graded sandstone, siltstone and tuff, grey laminated mudstone and grey to white, laminated to thinly bedded tuff; (3) greenish to pinkish grey, crudely bedded to massive tuff alternating with grey, laminated to horizontally bedded lacustrine deposits, yielding abundant fossils of insects, clam shrimps, plants and rare vertebrates.

Previous research showed that most Yanliao fossils were recovered from the laminated lacustrine deposits of Unit 3 (Sullivan et al., 2014; Cheng et al., 2015; Luo et al., 2015) (Fig. 2A). Poorly preserved fossils of bivalves, anostracans, clam shrimps, insects and plants have also been reported from rare laminated mudstone intercalations in Unit 1 (Huang et al., 2015).

4.2 Depositional environments

4.2.1 Petrology

The classification of the volcaniclastic rocks in this paper follows Schmid (1981).

Sediments of the Daohugou Beds are mostly volcaniclastics, consisting mainly of angular crystals of quartz and vitric shards, with minor plagioclase, biotite and pumice, and rare scoria and juvenile lithics in a vitric or argillaceous matrix (Figs. 3 and 4). Vitric grains are usually blocky or platy in shape, exhibiting low vesicularity and sometimes moss-like surface texture, with minor Y-shaped bobble wall shards, and fine- to extremely fine-grained (mostly 20–60 μm wide) (Figs. 3B–C and 4B–D). The dominance and fine grain size of the angular volcaniclasts, and the morphology of the vitric grains, suggest that the eruptions were mainly phreatomagmatic (Heiken, 1972; Self, 1983; Wohletz, 1983; Fisher and Schmincke, 2012).

233

Fig. 3 Sedimentary texture and structure of crudely bedded to massive tuff and breccia-bearing lapilli tuff (Lithofacies 1). A. Plant fragments (p) with preferred orientation, mudstone rip-ups (m), and juvenile lapilli (j); the coin is 19 mm in diameter. B–C. (B) Y-shaped and (C) blocky, platy vitric shards in an extremely fine-grained vitric matrix; note the separated vesicles in vitric grains (arrows in C); plane-polarized photomicrographs. D. Crudely parallel to cross bedding (arrow); the pencil is 15 cm long. E–F. Migrated channel-fill bedding (E) and close-up of the scoured underlying non-laminated mudstone (F, Lithofacies 5); note the rip-ups (arrows) derived from the red non-laminated mudstone; the coin is 19 mm in diameter. G. Large-scale slump of lacustrine deposits (dashed line) within the tuff; note the undisturbed lacustrine deposits underlying the tuff; the round signs are 17 cm in diameter. H. Outsized exotic boulder of mudstone (dashed line) within lapilli tuff-breccia; the hammer is 28 cm long. (For interpretation of the references to colour in this figure legend, the reader is referred to the web version of this article.)

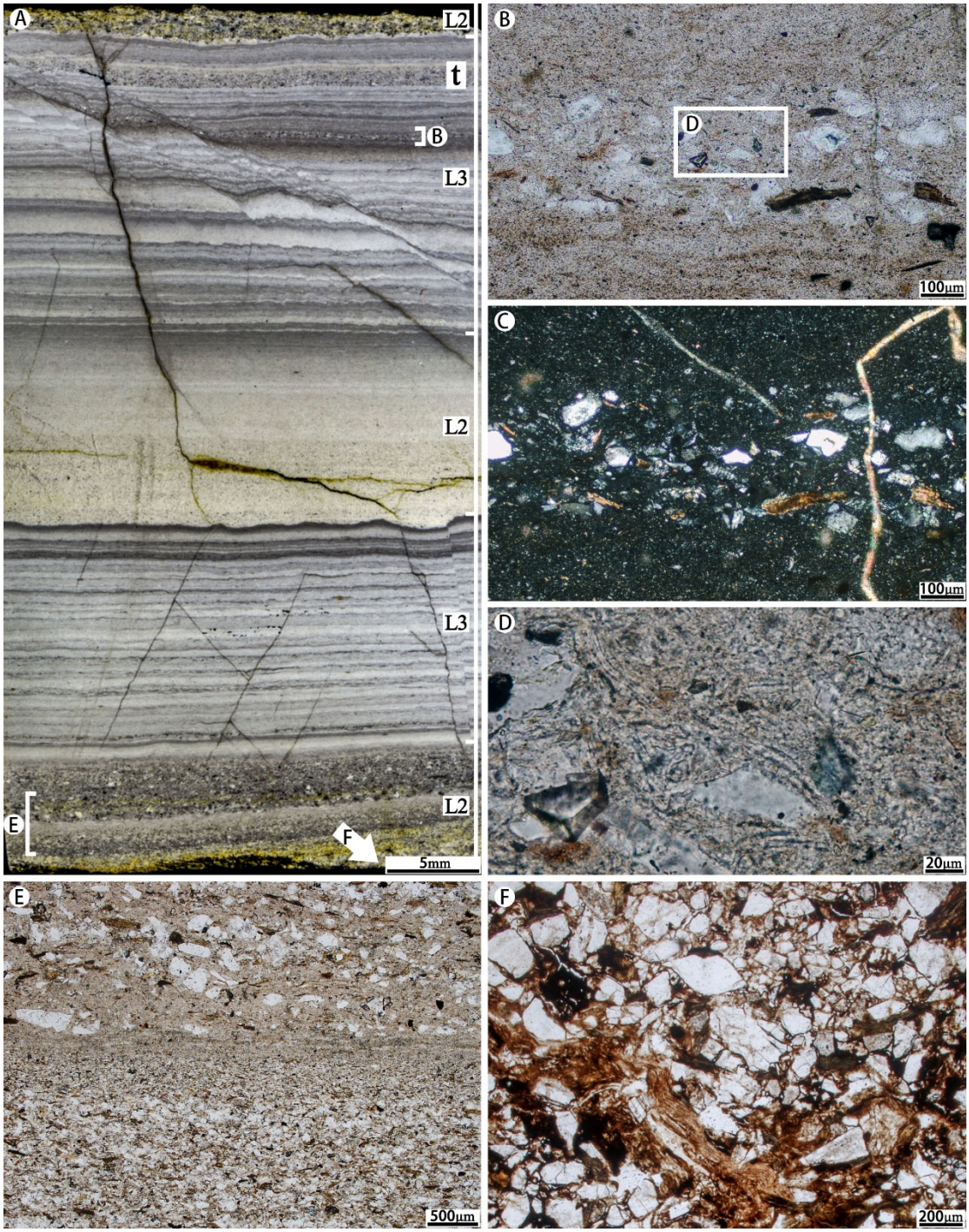

Fig. 4 Sedimentary texture and structure of graded sandstone, siltstone and tuff (Lithofacies 2) and laminated, normally graded siltstone, claystone and tuff (Lithofacies 3). A. A polished section from interval Π (stratigraphic position shown in Fig. 6A) shows alternation of the two lithofacies (L2 and L3) with intercalation of tuff lamina (t, Lithofacies 6). B–C. Plane-polarized and cross-polarized close-up views, respectively, of the narrow stratigraphic interval

marked in A shows the laminated, normally graded siltstone, claystone and tuff is mainly composed of vitric and crystal grains. D. Plane-polarized close-up view of the rectangle marked in B shows vitric grains are locally aligned parallel to margins of larger clasts. E–F. Plane-polarized close-up views at different scales of the narrow stratigraphic intervals marked in A show normal grading (E) and quenching (F) structures in the graded sandstone, siltstone and tuff.

The volcaniclastics underwent varying degrees of alteration. Devitrification is particularly common, indicated by fuzzy microcrystalline textures at, and close to, the margins of vitric grains (Figs. 3B–C and 4B–D) (Lofgren, 1971; Streck and Grunder, 1995). X-ray diffraction (XRD) analysis (Supplementary material Appendix 1–2) on the fossil-bearing mudstone from Unit 3 reveals a mean composition including 21.5% montmorillonite and 16.5% illite, reflecting montmorillonitization and subsequent illitization of vitric grains (Fisher and Schmincke, 2012; Huff, 2016), and 22.5% vermiculite, probably weathered from biotite (Pozzuoli et al., 1992).

Pyroclastic flows generated subaerially but deposited subaqueously resemble flows generated by re-sedimentation of fresh volcanic materials in both sediment composition and flow behaviour and thus may produce almost identical deposits, especially for low-temperature and distal pyroclastic flows (Whitham, 1989; Mandeville et al., 1996; Fisher and Schmincke, 2012). The Daohugou volcaniclastics may thus include both pyroclastic and epiclastic deposits. Regardless of their origins, however, we categorize these sediments together in two lithofacies: graded sandstone, siltstone and tuff, and laminated, normally graded siltstone, claystone and tuff. This categorization is based solely on the common

mechanism of sediment transport, i.e. subaqueous density flow and suspension.

4.2.2 Lithofacies

We recognize six lithofacies in the Daohugou Beds (Table 1).

	Lithofacies	Description	Interpretation	Facies associations*		
				Volcaniclastic apron	Fan delta	Lake floor
1	Crudely bedded to massive tuff and breccia-bearing lapilli tuff	Crudely parallel-, cross-, channel-fill bedded or massive; poorly sorted; ungraded or normally graded; oriented carbonized plant debris; up to 4 m thick	Pyroclastic flow	D	A	
2	Graded sandstone, siltstone and tuff	Parallel- or cross-bedded to laminated; normally graded; soft sediment deformation; preferred orientation of plant debris; non- to moderately fossiliferous; millimetres to centimetres thick	Transformed subaqueous pyroclastic flow and hyperpycnal flow		D	P
3	Laminated, normally graded siltstone, claystone and tuff	Planar-laminated; moderately to well sorted; normally graded; small-scale syndepositional deformation; highly fossiliferous; laminae 100 μm–3 mm thick	Suspended-load-dominated hyperpycnal flow		A	D
4	Laminated, rhythmic siltstone and claystone	Planar-laminated; moderately to well sorted; normally graded or structureless; couplets of clay-poor and clay-rich laminae; moderately to highly fossiliferous; laminae 30–700 μm thick	Suspension and distal turbidity current		P	A
5	Non-laminated mudstone	Stratified; moderately to poorly sorted; normally graded or structureless; non- to moderately fossiliferous; centimetres to decimetres thick	Suspension and distal turbidity current		P	
6	Laminated to thinly bedded tuff	Stratified to laminated; moderately to well sorted; normally graded; non- to moderately fossiliferous; millimetres to decimetres thick	Subaqueous ash fall		A	A

*D = dominant; A = associated; P = present.

Table 1 Lithofacies and facies associations in the Daohugou Beds

4.2.2.1 Lithofacies 1: crudely bedded to massive tuff and breccia-bearing lapilli tuff. This

lithofacies can be massive or can show crude parallel-, cross-, or channel-fill bedding, and ranges in thickness from several decimetres to nearly four metres (Fig. 3). The sediments are poorly sorted and occasionally normally graded. Carbonized land plant fragments (up to 0.5 m long) are common (Fig. 3A). Elongated clasts and plant fragments are typically aligned parallel to bedding and often show preferred orientation (Fig. 3A). Vesicles are present as subspherical voids less than 1 mm wide. Irregularly-shaped rip-up clasts of mudstone (cm to dm long) are occasional features at the bases of beds (Fig. 3A, E–F). Accidental lithics (typically 10–30 mm, maximum 2.7 m wide), consist mainly of tuff, granite and mudstone (Fig. 3H) and are rich in lapilli tuff-breccia from Unit 1 (Fig. 2A).

The crude stratification and poor sorting seen in this lithofacies, and the preferred orientation of carbonized plant fragments and elongate clasts, are characteristic of pyroclastic flow deposits (Buesch, 1992; Branney and Kokelaar, 2002; Fisher and Schmincke, 2012). The carbonized plant fragments were probably engulfed when the flows passed over vegetation, as in modern pyroclastic flows (Hudspith et al., 2010). The presence of mudstone rip-ups and channel-fill bedding in the basal part of some tuffs indicate the initial flows may have been subaqueous and scoured unconsolidated lacustrine deposits (Whitham, 1989; Mandeville et al., 1996), whereas the absence in the overlying tuffs of evidence for subaqueous transport, such as lamination, sorting, grading, or presence of aquatic fossils, could reflect a shift to subaerial deposition of the subsequent flows. The presence of out-sized boulders of country rock in Unit 1 suggests the deposits were formed proximal to phreatomagmatic eruptions accompanied by syneruption landslides, lahars or vent-clearing explosions (Belousov and Belousova, 2001; Hungr et al., 2001; Manville et al., 2009).

306 *4.2.2.2 Lithofacies 2: graded sandstone, siltstone and tuff.* This lithofacies consists of
307 horizontal-, wavy- and cross-stratified, moderately sorted, normally graded sandstone, sandy
308 siltstone and siltstone (Figs. 4A, E–F and 6). Strata are usually 0.35–300 mm thick, with a
309 sharp, sometimes erosive base, uneven top and lateral variations in thickness (Figs. 4A and 6).
310 Clasts can exhibit a jigsaw fracture pattern, a branching network of cracks on the clast
311 surfaces or cutting through individual clasts (Fig. 4F). Plant debris is common, as are
312 syndepositional deformational structures, such as load casts, rip-up clasts, convolute bedding
313 and slump structures (Figs. 3G, 4A and 6).

314 This lithofacies resembles flood deposits generated by hyperpycnal flows (e.g. Kassem
315 and Imran, 2001; Mulder and Alexander, 2001; Alexander and Mulder, 2002; Chapron et al.,
316 2007). The dominant fresh volcaniclastic component of the sediments suggests that the flows
317 represent either influxes of surface runoff carrying recently erupted tephra or distal
318 subaqueous deposits of pyroclastic flows (Whitham, 1989; Mandeville et al., 1996; Mulder
319 and Alexander, 2001; Fisher and Schmincke, 2012). Part of the tephra may have remained
320 sufficiently hot at the site of deposition to produce the jigsaw-fractured clasts by quenching
321 fragmentation (Whitham, 1989; Büttner et al., 1999; Fisher and Schmincke, 2012).
322 *4.2.2.3 Lithofacies 3: laminated, normally graded siltstone, claystone and tuff.* This
323 lithofacies occurs mostly in the lower part of Unit 3 (Fig. 2A). It is moderately to well-sorted
324 and has normally graded laminae with sharp non-erosive bases and uneven tops (Figs. 4A–C
325 and 6). The laminae usually are 100 μm–3 mm thick, but thickness can vary laterally (Fig.
326 6D). Millimetre-scale soft-sediment deformation structures, including wavy lamination and
327 microfaults which locally penetrated and distorted a limited number of laminae (Figs. 4A and

328 6), are common. Vitric chips locally aligned parallel to the margins of larger clasts represent
329 possible welding structures (Fig. 4B–D).

330 The lithofacies shows characteristics of suspended-load-dominated hyperpycnal flow
331 deposits, such as normal grading, a sharp but non-erosive base and uneven top, common
332 small-scale syndepositional deformation structures, and closely associated deposits of graded
333 sandstone, siltstone and tuff (Sturm and Matter, 1978; Anderson et al., 1985; Mulder and
334 Chapron, 2011). The flow was very low-energy, failing to erode the lake floor, and deposited
335 sediments from buoyant plumes concordant to lake-floor topography (Chapron et al., 2007;
336 Ducassou et al., 2008). The occasional welding structure suggests that part of the tephra may
337 have been remained relatively hot at the site of deposition (Whitham, 1989; Fisher and
338 Schmincke, 2012).

339 *4.2.2.4 Lithofacies 4: laminated, rhythmic siltstone and claystone.* This lithofacies is
340 moderately to well-sorted and consists of laterally persistent couplets of clay-poor (dark) and
341 clay-rich (light) laminae (ca. 30–700 μm thick) with a clearly bimodal grain size distribution
342 (Fig. 5). Locally the clay-rich laminae exhibit a brown colour (Fig. 5B). This lithofacies
343 occurs as thin intercalations in Lithofacies 3, particularly at interval E in the North pit and
344 intervals 2, 13 and 16 in the South pit.

345 The lithofacies resulted from predominantly distal turbidity flow and suspension settling
346 (Sturm and Matter, 1978; Anderson et al., 1985; Nelson et al., 1986; Smith, 1986). The
347 couplet laminae probably reflect discontinuous accumulation of the biogenic and fine
348 terrigeneous particles, resembling couplets produced in modern seasonally stratified water
349 columns (Sturm and Matter, 1978; Sturm, 1979).

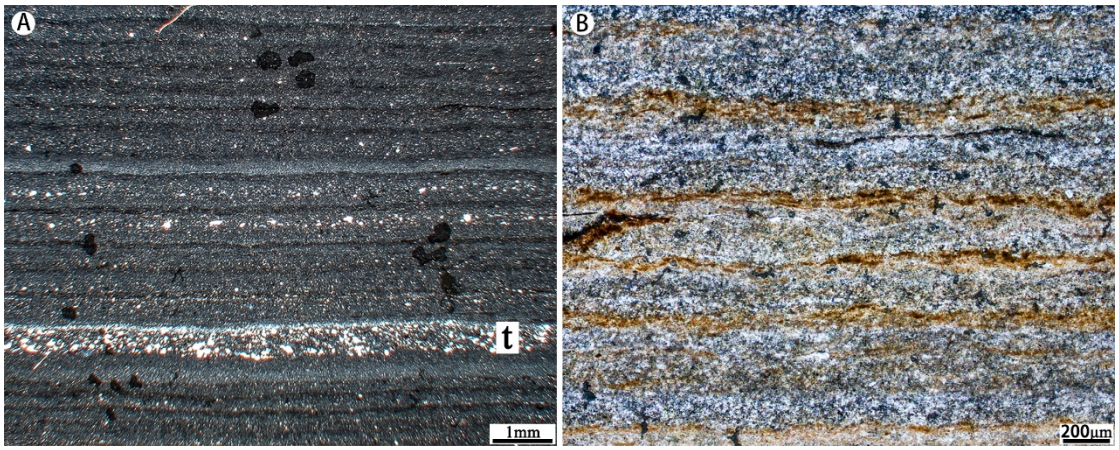

Fig. 5. Sedimentary texture and structure of laminated, rhythmic siltstone and claystone. A. Cross-polarized photomicrograph shows regular couplets of clay-rich (dark) and clay-poor (light) laminae interrupted by a tuff lamina (t, Lithofacies 6) from a stratigraphic interval exposed near South pit. B. Plane-polarized photomicrograph shows brown clay-rich couplet laminae; from interval 16 in South pit. (For interpretation of the references to colour in this figure legend, the reader is referred to the web version of this article.)

4.2.2.5 Lithofacies 5: non-laminated mudstone. This lithofacies occurs in the upper part of Unit 3 (Fig. 2A). It occurs as poorly to moderately sorted, normally graded or internally structureless beds 35 mm to ca. 0.8 m thick (Fig. 3E–F).

This lithofacies probably represents distal turbidity flow and suspension deposits (Chun and Chough, 1995; Larsen and Crossey, 1996). The lack of internal structure may reflect extensive bioturbation or rapid deposition of suspended sediment (Sturm, 1979; Reineck and Singh, 2012).

4.2.2.6 Lithofacies 6: laminated to thinly bedded tuff. This lithofacies occurs as frequent, irregular intercalations of laminae or minor thin beds (200 μm–200 mm thick) in Lithofacies

2–4 (Figs. 5A and 6C). It is laterally persistent with a sharp base and gradual upper contact, fine to extremely fine-grained, and normally graded with a vitric-rich top (Figs. 5A and 6C). Small plant fragments are common.

This lithofacies is interpreted as subaqueous ash fall deposits based on the dominance of crystal and vitric particles as well as its lateral persistence, associated subaqueous deposits, sharp basal contact and gradual upper contact, and normal grading (Niem, 1977; Allen and Cas, 1998; Fisher and Schmincke, 2012).

4.2.3 Facies associations

The six lithofacies form three facies associations that characterize distinct palaeoenvironments: volcaniclastic apron, fan delta and lake floor (Table 1).

The volcaniclastic apron comprises Lithofacies 1, i.e. pyroclastic flow deposits associated with proximal fallout and eruption-related lahar deposits (Smith, 1988, 1991; Riggs and Busby-Spera, 1990). The presence of outsized boulders of mudstone in the basal part of the sequence reflects initial vent-clearing explosions that probably occurred when rising magma interacted with water-saturated sediments (Wilson and Walker, 1985; Belousov and Belousova, 2001).

The fan delta is characterized by Lithofacies 2 in association with Lithofacies 1, 3 and 6, with a minor component of Lithofacies 4 and 5. The closely associated deposits arising from subaerial pyroclastic flow, subaqueous ash fall, hyperpycnal flow and suspension reflect a fan delta environment subject to significant influx of fresh volcaniclastic sediments (Nemec and Steel, 1988; Whitham, 1989; Horton and Schmitt, 1996; Mandeville et al., 1996).

The lake floor comprises mainly Lithofacies 3 in association with Lithofacies 4 and 6, with a minor component of Lithofacies 2. The dominance of distal turbidity current and suspension deposits, together with the abundance of aquatic fossils, suggest a lake floor environment of the kind typically found in the low-energy central basins of temperate lakes (Sturm and Matter, 1978; Nelson et al., 1986; Reineck and Singh, 2012), based on the dominance of sediments formed by hyperpycnal flow. Frequent intercalations of tuff laminae or thin beds indicate that frequent volcanic eruptions occurred in the area.

4.3 Community composition and fossil preservation

Most fossils are preserved in laminated mudstone (Lithofacies 3 and 4), although rare aquatic fossils, especially clam shrimps, also occur scattered in Lithofacies 2, 5 and 6, and occasionally in Lithofacies 1 (Figs. 2A and 6). With rare exceptions (clam shrimps preserved in three-dimensions in Lithofacies 2 and 5), most fossils are preserved in two dimensions with their ventrodorsal or lateral surfaces parallel to the bedding planes.

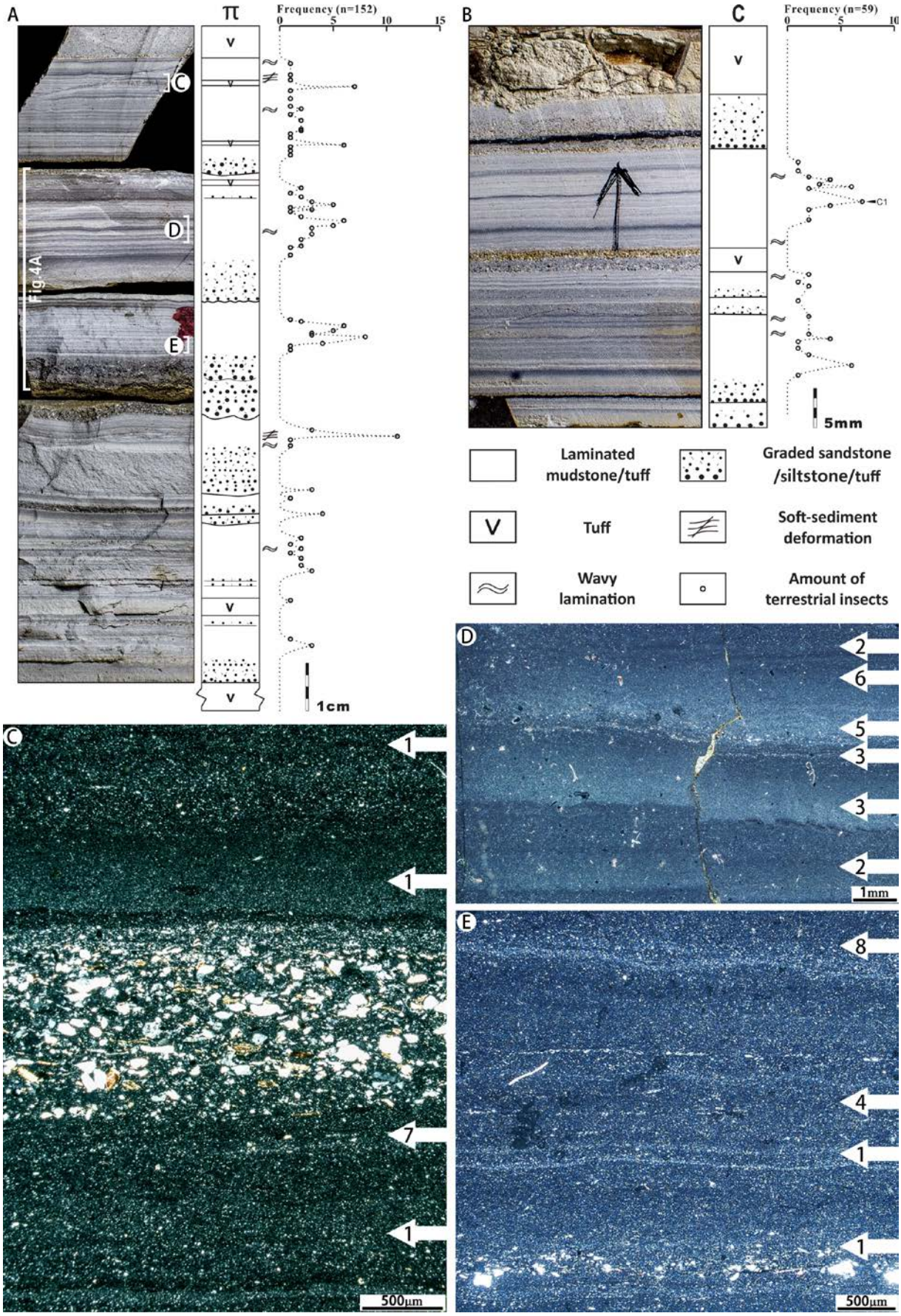

405

406 **Fig. 6.** Occurrences and abundance of terrestrial insects. A–B. Polished sections show

407 stratigraphic successions and numbers of uncovered terrestrial insects for various horizons
408 within the fossiliferous intervals Π (A) and C (B) from the North pit; a few specimens (5 and
409 4 from Π and C intervals, respectively; see Fig. 2A) were not included due to uncertainty
410 regarding their exact occurrence horizons. C–E. Cross-polarized photomicrographs of the thin
411 sections from the horizons marked in A show the horizons in more detail, and the number of
412 terrestrial insects found in each horizon.
413
414 Benthic aquatic organisms are abundant, but of low diversity. Only four species were
415 identified (Wang et al., in prep.): the clam shrimp *Triglypta haifanggouensis*, recently
416 reviewed by Liao et al. (2017); larvae of the mayfly *Fuyous gregarious* and *Shantous*
417 *lacustris*; and the water boatman *Daohugocorixa vulcanica*. Clam shrimps are the dominant
418 benthic aquatic group and occur in all fossiliferous horizons, with a density of over 1000/m^2
419 in 31 of the 35 quantitatively studied horizons. They can be extremely concentrated in
420 Lithofacies 4, with a density of up to 14487/m^2 (extrapolated from measurement of an 81.45
421 cm^2 surface). Mayfly larvae and water boatmen are less common. Mayfly larvae occur in 25
422 of the 35 quantitatively studied horizons, with a density of up to 421/m^2 (extrapolated from
423 measurement of a 284 cm^2 surface), and water boatmen exist in 21 horizons with a density of
424 up to 251/m^2 (extrapolated from measurement of a 636 cm^2 surface) (Wang et al., in prep.).
425 Most of these fossils are articulated with little fragmentation and typically retain delicate
426 details such as carapace ornamentation (clam shrimps), tergalii and cerci (mayfly larvae), and
427 setae (water boatmen).
428 Terrestrial animals are represented exclusively by insects and are rare in the South pit

(only 14 specimens were recovered in four horizons; Fig. 2A). In contrast, insects are abundant in the North pit, in which 380 specimens representing 15 orders and 57 families were collected from 11 intervals (Fig. 2A). Among these, 54.9% of specimens are edaphic taxa, 37.3% sylvan, and 7.8% alpine (Wang et al., in prep.). Most terrestrial insects are preserved in Lithofacies 3 that forms many thin intervals (ca. 7–28 mm thick) with deposits of lithofacies 2 in between (Figs. 2, 4 and 6). Within each interval the insects occur in many laminae associated with abundant aquatic organisms, but are particularly abundant in some laminae that directly underlie tuff of fallout origin (Fig. 6). The associated fossils of aquatic insects sometimes show preferred plan-view orientation (e.g. horizons B2, C1, F1 and I3, Supplementary material Appendix 2). Most terrestrial insects are well preserved: over 50% of the specimens are complete and articulated, and various fine anatomical details are preserved (e.g., cerci, filiform antennae, tiny spines and setae) (Wang et al., in prep.).

Similarly, terrestrial plants are rare in the South pit (only five specimens were found) but more abundant in the North pit (114 specimens were recovered from the 11 fossiliferous intervals mentioned above (Fig. 2A)). The plants include ferns, caytonialeans, bennettites, ginkgophytes, czekanowskialeans and conifers. Among these, tall-growing gymnosperms are dominant, preserving entire or large fragments of leaves and organs, while water- or moisture-bound groups such as ferns are represented by only rare fragmentary remains (Pott and Jiang, 2017).

5. Discussion

5.1 Depositional model

In the studied area, the lake floor and fan delta deposits are very thin, ranging from ca. 0.2 to 1 m thick, while the volcaniclastic apron deposits, which sandwich successive lacustrine intervals, are often much thicker (up to at least 4.4 m thick) (Fig. 2A; e.g. intervals 11–13 in Museum section). This distribution of lacustrine and volcaniclastic apron deposits indicates that the lacustrine sediments formed on, and were derived mainly from, volcaniclastic apron deposits that directly underlie them (Figs. 2 and 7).

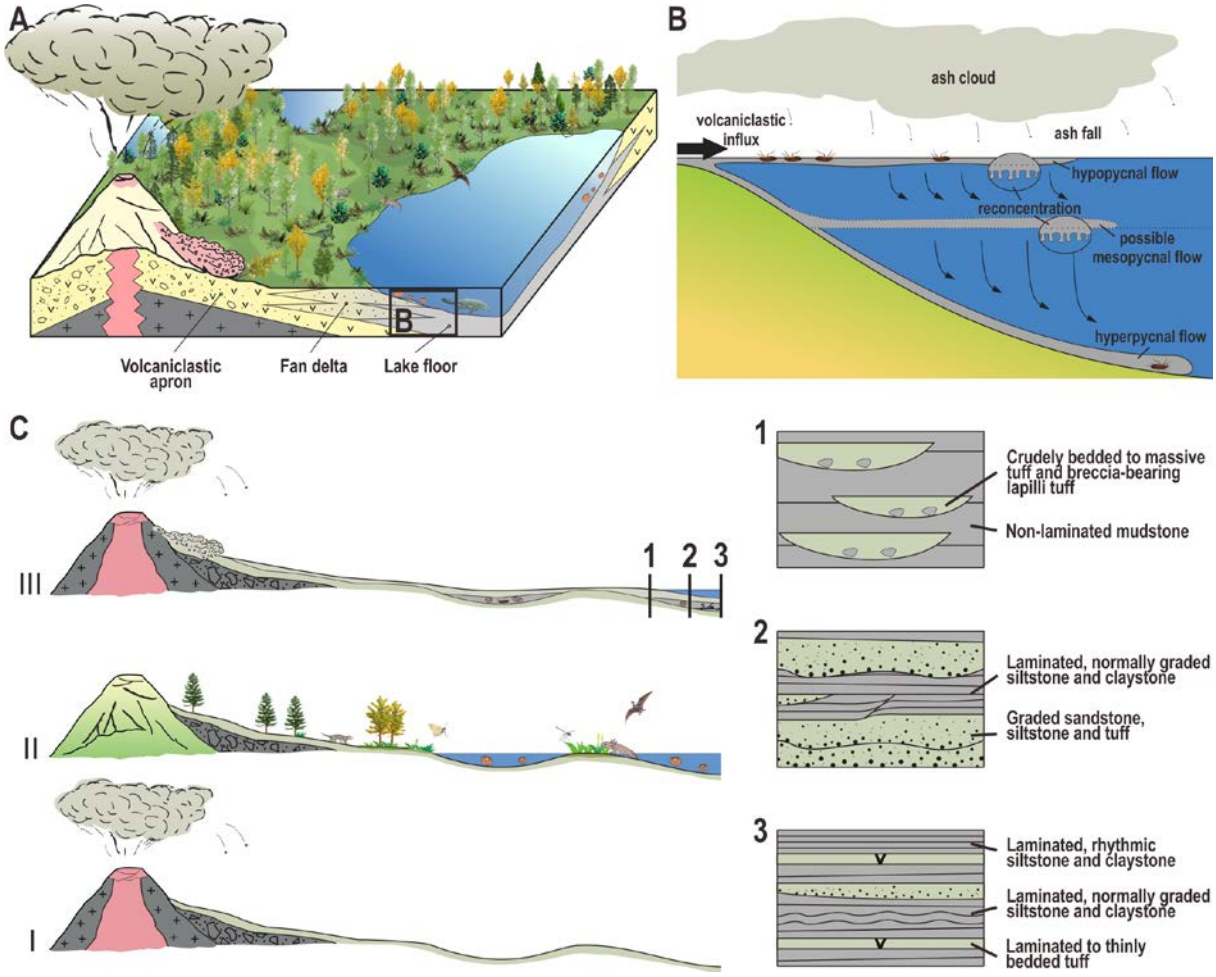

Fig. 7. A–B. Depositional model of the Daohugou Beds in the studied area (A), and

460 biostratinomic model of the land animal remains (B). C. Illustrative sketch (not to scale) of
461 the evolution of the Daohugou lake(s): I–II, waterbodies gradually accumulated on the
462 volcaniclastic apron, where the Daohugou ecosystem was established and developed; II–III,
463 during syneruption periods, volcaniclastic influxes repeatedly devastated the ecosystem and
464 buried the remains, and may even have destroyed the lake completely; keys as in Figs. 2 and
465 3. Some of the animal figures were revised from reconstructions by Rongshan Li, Nobu
466 Tamura and April M. Isch.

467 There are two scenarios that could account for this frequent alternation of thin lacustrine
468 deposits and thick volcaniclastic apron deposits. The studied section could represent
469 deposition in marginal regions of a single lake, with the frequent influxes of volcaniclastic
470 apron material causing substantial fluctuations in lake area and resulting in the frequent and
471 abrupt lateral alternation of the two facies. The lake would necessarily have had steep margins
472 with restricted development of marginal facies in littoral and shallow-water zones, at least at
473 the studied sites, because there is no evidence for typical shallow-water wave activity such as
474 wave-formed ripples or cross-stratification. The influxes of volcaniclastic material, including
475 remobilized sediments on the marginal slope, may have frequently disturbed the underlying
476 lacustrine deposits and formed the observed large mudstone rip-ups and slump structures
477 (Figs. 3A, E–G and 6).

478 Alternatively, many comparatively short-lived lakes could have developed on the
479 volcaniclastic apron in the studied area, as commonly seen in modern analogues (Anderson et
480 al., 1985; Blair, 1987a; Manville et al., 2001; Dale et al., 2005; Christenson et al., 2015).
481 These lakes may have been filled up with volcaniclastic material or breached, as a result of

damage to their shorelines from volcanic eruptions, and then covered by volcaniclastic apron sediments arising from subsequent eruptions. The extensive disturbance of the lacustrine deposits (Figs. 3A, E–G and 6) may then have resulted from the process of filling or breaching the lakes, similar to the final lake-fill sequence in the Eocene Challis volcanic field, where extensive pyroclastic deposits filled a ca. 20 m deep intermontane lake (Palmer and Shawkey, 1997, 2001). The fine-textured tephra from the top of the volcaniclastic apron deposits would have formed a water-tight surface crust after wetting (Dale et al., 2005), upon which another cycle of lake sediments accumulated (Fig. 7C).

It remains unclear which scenario applies here given the uncertainty about the basin structure and lake topography. Nonetheless, in either case the hydrological regime clearly changed frequently and rapidly at the studied sites, causing the repeated and abrupt shifts from volcaniclastic apron deposits to lacustrine deposits. This may be ascribed to damming of the drainage network and subsequently shaping new lakes or raising water level of pre-existing lakes by the emplacement of volcanic materials, as occurs in modern and recent counterparts to this depositional system (Scott et al., 1996; Simon, 1999; Palmer and Shawkey, 1997, 2001). Active earthquakes and fault movements in the Daohugou area associated with volcanism or tectonics (Liu et al., 2004; Y. Zhang et al., 2008; Huang, 2015) may also have created areas of low topography, disrupting groundwater and surface-water systems (Blair, 1987b; Palmer and Shawkey, 1997, 2001).

5.2 Biostratinomic model

The high abundance of aquatic taxa in the lacustrine deposits reflects a combination of

high population densities and time averaging, especially in the laminated, rhythmic siltstone and claystone (Lithofacies 4) where clam shrimps occurred in extremely high density while land animals were rare. In contrast, aquatic animals with repeated association of high concentrations of terrestrial insects of different niches and various ontogenetic stages (Liu et al., 2010) in laminated, normally graded siltstone, claystone and tuff (Lithofacies 3), might suggest repeated mass mortality events in the area. The dominant fresh volcaniclastic component of the host sediments and very limited decay of the carcasses before burial (Martínez–Delclòs and Martinell, 1993; Duncan et al., 2003; Wang et al., 2013) suggest that the mass mortality events occurred during, and were probably associated with, volcanic eruptions, resembling similar events resulting from more recent and modern eruptions (Baxter, 1990; Dale et al., 2005; Christenson et al., 2015; Zhou et al., 2016).

The close association of the terrestrial-insect-fossil-bearing laminae (Lithofacies 3) with graded sandstone, siltstone and tuff (Lithofacies 2), indicates that these land animal remains were probably transported into the lake(s) by influxes of fresh volcaniclastic material. Transport of terrestrial vertebrates with complete skeletons and extensive soft tissue preservation into lacustrine environments has been linked to high-temperature pyroclastic flow (Jiang et al., 2014). Evidence for hot emplacement in Lithofacies 2 and 3, however, is scarce, suggesting that transport mainly involved runoff during high discharge periods associated with eruptions and possibly minor distal low-temperature pyroclastic flows (Sigurdsson et al., 1982); such flows carried newly erupted tephra and remains of terrestrial organisms that were engulfed into the flows into the lake(s), and triggered subaqueous density flows due to the density contrast between the flows and ambient lake water.

As commonly observed in taphonomic experiments, most freshly killed insects remain floating on the water surface in a still water body until significant decay occurs (e.g. Martínez-Delclòs and Martinell, 1993; Duncan et al., 2003; Wang et al., 2013). Indeed, the Daohugou fossils probably drifted far offshore (Fig. 7B), as indicated by the accompanying plant fossil assemblage, which mostly comprises large land plants but includes some low-growing water-related plants (Pott and Jiang, 2017). The abundance and high fidelity of preservation of insects, however, probably reflects minimal flotation prior to burial. Such rapid sinking may be attributed to turbulent water caused by wind or continuing subaqueous density flow (Martínez-Delclòs and Martinell, 1993), but this conflicts with our evidence that the laminae hosting terrestrial insect fossils (Lithofacies 3) mostly resulted from very low-energy flows in which suspension processes represented the dominant form of deposition. Rather, these thin fossiliferous intervals may reflect repeated processes of rapid settling of fine-grained sediment particles and the floating remains, by convective sedimentation. In other words, successive reconcentrations of settling particles within overflow or concentrations of ash fall in the surface water built up the convective instability of the surface layer; this increasing instability then triggered fast-descending convective plumes, forming vertical gravity currents that entrained the remains, and eventually reached the lake floor and generated the very low-energy hyperpycnal flows (Sturm and Matter, 1978; Carey, 1997; Parsons et al., 2001; Ducassou et al., 2008; Davarpanah and Wells, 2016) (Fig. 7B). This process may result in sedimentation rates one to three orders of magnitude greater than the Stokes settling velocity (Carey, 1997; Davarpanah and Wells, 2016), and thus probably sealed the remains in a timely fashion and protected them from further decay.

548 In addition, the occurrence of particularly fossiliferous laminae directly underlying tuff
549 laminae (Fig. 6A and C) may indicate that, even if the ash fall was not concentrated enough to
550 trigger convective sedimentation, it could nevertheless have caused rapid sinking and burial
551 simply by settling on the dead animals and adding to their weight (Tian et al., in prep.).
552
553 5.3 Palaeoenvironmental implications
554 The stratigraphic succession shows that intense volcanic eruptions produced extensive
555 volcaniclastic apron deposits in the studied area. One or more lakes developed on the
556 volcaniclastic apron and were subject to frequent influxes of voluminous volcaniclastic
557 sediments (Fig. 7). The aquatic ecosystem of the lake(s) resembled that of modern short-lived
558 waterbodies in being characterized by a low-diversity aquatic fauna with a high population
559 density, dominated by crustaceans (clam shrimp *Triglypta haifanggouensis*) and pond-type
560 salamanders (Vannier et al., 2003; Liu et al., 2010; Sullivan et al., 2014). Although hatching
561 does not require a dry phase, clam shrimps produce eggs that may survive several years (to
562 decades) of drought (Dumont and Negrea, 2002). They disperse through water-, animal- and
563 wind transportation (Tasch, 1969; Webb, 1979; Frank, 1988), and might have easily endured
564 frequent collapses of the lacustrine ecosystem caused by volcanic eruptions. Their successful
565 dispersal strategies mean that clam shrimps would have been able to rapidly colonize newly-
566 established aquatic niches. Ephemerid nymphs and water boatmen were less abundant, and
567 they probably colonized the new post-eruption lake habitats by migrating from nearby
568 habitats (Batzer and Wissinger, 1996).
569 The longevity of the lake(s) is unclear, as the degree of ecological similarity between

these benthic aquatic taxa of the Haifanggou Formation and their modern relatives is uncertain. Although clam shrimp population palaeoecology has often been interpreted based on an analogy with the “shallow and temporary” habitats of extant members of this group (e.g., Frank, 1988; Vannier et al., 2003), their ancient analogues clearly occupied a much wider ecological space (Olsen, 2016; Hethke et al., submitted for publication). Particularly clam shrimps from the Jehol Biota, an Early Cretaceous counterpart of the Yanliao Biota from the same geographic region, were recently interpreted to have adapted to life in the perennial volcanic Lake Sihetun that went through an overall shallowing and a consequent shift from holomictic/meromictic to fully holomictic conditions (Hethke et al., submitted for publication). In addition, modern Corixidae can be early colonizers of temporary waters, but many species frequently appear in permanent ponds and lakes as well as streams (e.g. Brown, 1951; Jansson and Reavell, 1999). Further, mayfly nymphs occur in all sorts of water bodies, including shallow areas of deep permanent lakes (e.g. Lyman, 1943; Brittain and Sartori, 2009). The consistently low-diversity associations of clam shrimps, water boatmen and mayfly larvae might thus indicate small regional species richness in, and frequent disturbance of, a set of interconnected habitats (Chase, 2003); alternatively, they may reflect a lack of hydrological connectivity.

The presence of highlands surrounding the lake(s) is supported by extensive fan-delta deposits and the preservation of alpine insects and upland plants in the lacustrine deposits (Liu et al., 2010; Na et al., 2015; Na et al., 2017; Pott and Jiang, 2017). The relatively high abundance of land plant debris in pyroclastic flow deposits and the paucity of epiclasts derived from weathering suggest that the region adjacent to the lake(s) was well vegetated.

This is consistent with the warm and humid climate inferred from the nature of the Yanliao flora (Liu et al., 2010; Na et al., 2015; Na et al., 2017; Pott and Jiang, 2017).

Even though the present case study was based on the Daohugou area and mostly invertebrate fossils, it may have much wider application to the palaeoenvironment and biostratinomic pathways of the Yanliao Biota in other areas, since the fossil-bearing strata in all these areas share many characteristics. For instance, in most known localities, the Yanliao fossils were preserved in laminated lacustrine deposits, which frequently alternate with thick volcaniclastic apron deposits (Sullivan et al., 2014; Huang, 2015; Xu et al., 2016). The fossiliferous laminae in these localities are closely associated with normally graded siltstone, claystone and tuff according to our field observations. However, further investigation on the palaeoenvironment and biostratinomic features of the Yanliao Biota in other areas is needed to confirm the generality of our observations and interpretations.

6 Conclusions

Six lithofacies are recognized in the Daohugou Beds, and these form three facies associations in space and time: volcaniclastic apron, fan delta and lake floor. The stratigraphic succession shows that intense volcanic eruptions resulted in an extensive volcaniclastic apron and one or more lakes in the studied area. Thin lacustrine deposits frequently alternated with thick volcaniclastic apron deposits. This indicates either that the studied area was located in the marginal regions of a single lake, where frequent influxes of volcaniclastic apron material caused substantial fluctuations in lake area and thus the frequent lateral alternation of the two facies, or that many short-lived lakes developed on the volcaniclastic apron. Most terrestrial

insects were preserved in the laminated, normally graded siltstone, claystone and tuff facies that forms many thin intervals with deposits of graded sandstone, siltstone and tuff in between. Within each interval the terrestrial insects occur in many laminae associated with abundant aquatic organisms but are particularly abundant in some laminae that directly underlie tuff of fallout origin. Most of these terrestrial insects are interpreted to have been killed during volcanic eruptions. Their carcasses were dropped or transported by influxes of fresh volcaniclastic material, mostly comprising runoff but possibly including minor distal pyroclastic flow, into the studied lake(s). They then became rapidly buried before extensive decay could occur, probably due to a combination of rapid vertical settling, ash fall and water turbulence.

Acknowledgments

The authors thank Qi Zhang, He Wang, Miao Ge, and personnel of the Daohugou National Geopark for their kind support in the field. We are also deeply grateful to Dr. Christian Pott for identifying the plant fossils we collected, to Prof. Franz T. Fürsich, Prof. Frank Riedel and Prof. Volker Lorenz for constructive discussion and suggestions, and to Yingying Zhao for her great help with the drawings. This research was financially supported by the National Natural Science Foundation of China (41672010; 41688103; 41572010) and the Strategic Priority Research Program (B) of the Chinese Academy of Sciences (XDB26000000) to BYJ and BW, and by a European Research Council Starting Grant H2020–2014–ERC–StG–637698–ANICOLEVO awarded to MMN.

Data availability

Supplementary materials to this article can be found in the online version of the paper.

References

Alexander, J., Mulder, T., 2002. Experimental quasi–steady density currents. Mar. Geol. 186, 195–210.

Allen, S., Cas, R., 1998. Rhyolitic fallout and pyroclastic density current deposits from a phreatoplinian eruption in the eastern Aegean Sea, Greece. J. Volcanol. Geotherm. Res. 86, 219–251.

Anderson, R.Y., Nuhfer, E.B., Dean, W.E., 1985. Sedimentation in a blast-zone lake at Mount St. Helens, Washington—implications for varve formation. Geology 13, 348–352.

Büttner, R., Dellino, P., Zimanowski, B., 1999. Identifying magma-water interaction from the surface features of ash particles. Nature 401, 688–690.

Batzer, D.P., Wissinger, S.A., 1996. Ecology of insect communities in nontidal wetlands. Annu. Rev. Entomol. 41, 75–100.

Baxter, P.J., 1990. Medical effects of volcanic eruptions. Bull. Volcanol. 52, 532–544.

Belousov, A., Belousova, M., 2001. Eruptive process, effects and deposits of the 1996 and the ancient basaltic phreatomagmatic eruptions in Karymskoye lake, Kamchatka, Russia. Volcanogenic sedimentation in lacustrine settings. Int. Ass. Sedimentol. Spec. Publ. 30, 35–60.

Bi, S., Wang, Y., Guan, J., Sheng, X., Meng, J., 2014. Three new Jurassic euharamiyidan species reinforce early divergence of mammals. Nature 514, 579–584.

Blair, T.C., 1987a. Sedimentary processes, vertical stratification sequences, and geomorphology of the Roaring River alluvial fan, Rocky Mountain National Park, Colorado. J. Sediment. Res. 57, 1–18.

Blair, T.C., 1987b. Tectonic and hydrologic controls on cyclic alluvial fan, fluvial, and lacustrine rift–basin sedimentation, Jurassic–Lowermost Cretaceous Todos Santos Formation, Chiapas, Mexico. J. Sediment. Res., 57, 845–862.

Branney, M.J., Kokelaar, B.P., 2002. Pyroclastic density currents and the sedimentation of ignimbrites. Geol. Soc. Lond. Mem. 27, 1–143.

Brittain, J.E., & Sartori, M., 2009. Ephemeroptera (Mayflies). In Encyclopedia of Insects (Second Edition), pp. 328–334.

Brown, E.S., 1951. The relation between migration-rate and type of habitat in aquatic insects, with special reference to certain species of Corixidae. J. Zool. 121, 539–545.

Buesch, D.C., 1992. Incorporation and redistribution of locally derived lithic fragments within a pyroclastic flow. Geol. Soc. Am. Bull. 104, 1193–1207.

Cai, C., Thayer, M.K., Engel, M.S., Newton, A.F., Ortega-Blanco, J., Wang, B., Wang, X., Huang, D., 2014. Early origin of parental care in Mesozoic carrion beetles. Proc. Natl. Acad. Sci. U. S. A. 111, 14170–14174.

Carey, S., 1997. Influence of convective sedimentation on the formation of widespread tephra fall layers in the deep sea. Geology 25, 839–842.

Chapron, E., Juvigné, E., Mulsow, S., Ariztegui, D., Magand, O., Bertrand, S., Pino, M., Chapron, O., 2007. Recent clastic sedimentation processes in Lake Puyehue (Chilean Lake District, 40.5 S). Sediment. Geol. 201, 365–385.

680 Chase, J.M., 2003. Community assembly: when should history matter? Oecologia 136, 489–
681 498.
682 Chen, W., Ji, Q., Liu, D., Zhang, Y., Song, B., Liu, X., 2004. Isotope geochronology of the
683 fossil-bearing beds in the Daohugou area, Ningcheng, Inner Mongolia. Regional Geol.
684 China 23, 1165–1169.
685 Cheng, X., Wang, X., Jiang, S., Kellner, A.W., 2015. Short note on a non-pterodactyloid
686 pterosaur from Upper Jurassic deposits of Inner Mongolia, China. Hist. Biol. 27, 749–754.
687 Christenson, B., Németh, K., Rouwet, D., Tassi, F., Vandemeulebrouck, J., Varekamp, J.C.,
688 2015. Volcanic Lakes. Springer, Berlin, Heidelberg.
689 Chun, S., Chough, S.K., 1995. The Cretaceous Uhangri formation, SW Korea: lacustrine
690 margin facies. Sedimentology 42, 293–322.
691 Dale, V.H., Swanson, F.J., Crisafulli, C.M., 2005. Disturbance, survival, and succession:
692 understanding ecological responses to the 1980 eruption of Mount St. Helens. In: Dale
693 V.H., Swanson F.J., Crisafulli C.M. (Eds.), Ecological responses to the 1980 eruption of
694 Mount St. Helens. New York, NY: Springer; 2005. pp. 3–11.
695 Davarpanah Jazi, S., Wells, M.G., 2016. Enhanced sedimentation beneath particle-laden flows
696 in lakes and the ocean due to double-diffusive convection. Geophys. Res. Lett. 43, 10883–
697 10890.
698 Davis, G.A., Wang, C., Zheng, Y., Zhang, J., Zhang, C., Gehrels, G., 1998. The enigmatic
699 Yinshan fold-and-thrust belt of northern China: new views on its intraplate contractional
700 styles. Geology 26, 43–46.
701 Ducassou E., Mulder T., Migeon S., et al., 2008. Nile floods recorded in deep Mediterranean

sediments. Quat. Res. 70, 382–391.

Dumont, H.J. and Negrea, S.V. 2002. *Introduction to the Class Branchiopoda*. Leiden: Backhuys.

Duncan, I.J., Titchener, F., Briggs, D.E.G., 2003. Decay and disarticulation of the cockroach: implications for preservation of the blattoids of Writhlington (Upper Carboniferous), UK. Palaios 18, 256–265.

Fisher, R.V., Schmincke, H.-U., 2012. Pyroclastic rocks. Springer Science & Business Media.

Frank, P., 1988. Conchostraca. Palaeogeogr. Palaeoclimatol. Palaeoecol. 62, 399–403.

Gao, K., Chen, J., Jia, J., 2013. Taxonomic diversity, stratigraphic range, and exceptional preservation of Juro–Cretaceous salamanders from northern China. Can. J. Earth Sci. 50, 255–267.

Gao, K., Shubin, N.H., 2003. Earliest known crown-group salamanders. Nature 422, 424–428.

He, H., Wang, X., Zhou, Z., Zhu, R., Jin, F., Wang, F., Ding, X., Boven, A., 2004. $^{40}Ar/^{39}Ar$ dating of ignimbrite from Inner Mongolia, northeastern China, indicates a post-Middle Jurassic age for the overlying Daohugou Bed. Geophys. Res. Lett. 31, 1–4.

Heiken, G., 1972. Morphology and petrography of volcanic ashes. Geol. Soc. Am. Bull. 83, 1961–1988.

Hethke, M., Fürsich, F.T., Jiang, B., Wang, B., Chellouche, P., Weeks, S.C. submitted. Ecological stasis in Spinicaudata (Crustacea, Branchiopoda)? – Early Cretaceous clam shrimp of the Yixian Formation of NE China occupied a broader realized ecological niche than extant members of the group, 2018, (submitted for publication).

Horton, B.K., Schmitt, J.G., 1996. Sedimentology of a lacustrine fan‐delta system, Miocene

724 Horse Camp Formation, Nevada, USA. Sedimentology 43, 133–155.
725 Huang, D., 2015. Yanliao biota and Yanshan movement. Acta Palaeontol. Sin. 54, 501–546.
726 Huang, D. (Ed.), 2016. The Daohugou Biota. Shanghai Science and Technical Publishers,
727 Shanghai, 332 pp.
728 Huang, D., Engel, M.S., Cai, C., Wu, H., Nel, A., 2012. Diverse transitional giant fleas from
729 the Mesozoic era of China. Nature 483, 201–204.
730 Huang, D., Nel, A., Shen, Y., Selden, P., Lin, Q., 2006. Discussions on the age of the
731 Daohugou fauna-evidence from invertebrates. Progr. Nat. Sci. 16, 309–312.
732 Huang, D., Cai, C., Jiang, J., Yi-Tong, S.U., Liao, H., 2015. Daohugou bed and fossil record
733 of its basal conglomerate section. Acta Palaeontol. Sin. 54, 501–546.
734 Hudspith, V.A., Scott, A.C., Wilson, C.J., Collinson, M.E., 2010. Charring of woods by
735 volcanic processes: an example from the Taupo ignimbrite, New Zealand. Palaeogeogr.
736 Palaeoclimatol. Palaeoecol. 291, 40–51.
737 Huff, W.D., 2016. K-bentonites: a review. Am. Mineral. 101, 43–70.
738 Hungr, O., Evans, S., Bovis, M., Hutchinson, J., 2001. A review of the classification of
739 landslides of the flow type. Environ. Eng. Geosci. 7, 221–238.
740 Jansson, A., Reavell, P.E., 1999. North American species of Trichocorixa (Heteroptera:
741 Corixidae) introduced into Africa. Afr. Entomol. 7, 295–297.
742 Ji, Q., Luo, Z., Yuan, C., Tabrum, A.R., 2006. A swimming mammaliaform from the Middle
743 Jurassic and ecomorphological diversification of early mammals. Science 311, 1123–1127.
744 Jiang, B., 2006. Non-marine Ferganoconcha (Bivalvia) from the Middle Jurassic in Daohugou
745 area, Ningcheng County, Inner Mongolia, China. Acta Palaeontol. Sin. 45, 252–257.

746 Jiang, B., Harlow, G.E., Wohletz, K., Zhou, Z., Meng, J., 2014. New evidence suggests
747 pyroclastic flows are responsible for the remarkable preservation of the Jehol biota. Nat.
748 Commun. 5, 3151. http://dx.doi.org/10.1038/ncomms4151.
749 Jiang, B., Sha, J., 2006. Late Mesozoic stratigraphy in western Liaoning, China: a review. J.
750 Asian Earth Sci. 28, 205–217.
751 Kassem, A., Imran, J., 2001. Simulation of turbid underflows generated by the plunging of a
752 river. Geology 29, 655–658.
753 Kellner, A.W., Wang, X., Tischlinger, H., de Almeida Campos, D., Hone, D.W., Meng, X.,
754 2010. The soft tissue of *Jeholopterus* (Pterosauria, Anurognathidae, Batrachognathinae)
755 and the structure of the pterosaur wing membrane. Proc. R. Soc. Lond. B Biol. Sci. 277,
756 321–329.
757 Kidwell, S.M., Fuersich, F.T., Aigner, T., 1986. Conceptual framework for the analysis and
758 classification of fossil concentrations. Palaios 1, 228–238.
759 Larsen, D., Crossey, L.J., 1996. Depositional environments and paleolimnology of an ancient
760 caldera lake: Oligocene Creede Formation, Colorado. Geol. Soc. Am. Bull. 108, 526–544.
761 Li, Q., Clarke, J.A., Gao, K., Zhou, C., Meng, Q., Li, D., et al., 2014. Melanosome evolution
762 indicates a key physiological shift within feathered dinosaurs. Nature 507, 350-353.
763 Liao, H., Shen, Y., Huang, D., 2017. Conchostracans of the Middle–Late Jurassic Daohugou
764 and Linglongta beds in NE China. Palaeoworld 26, 317–330.
765 Liu, P., Huang, J., Ren, D., 2010. Palaeoecology of the Middle Jurassic Yanliao entomofauna.
766 Acta Zootaxon. Sin. 35, 568–584.
767 Liu, Y., Liu, Y., Zhang, H., 2006. LA-ICPMS Zircon U-Pb Dating in the Jurassic Daohugou

768 Beds and Correlative Strata in Ningcheng of Inner Mongolia. Acta Geol. Sin. (English
769 Edition) 80, 733–742.
770 Liu, Y., Liu, Y., Li, P., Zhang, H., Zhang, L., Li, Y., Xia, H., 2004. Daohugou biota-bearing
771 lithostratigraphic succession on the southeastern margin of the Ningcheng basin, Inner
772 Mongolia, and its geochronology. Region. Geol. Chin. 23, 1180–1187.
773 Lofgren G. Experimentally produced devitrification textures in natural rhyolitic glass. Geol.
774 Soc. Am. Bull. 82, 111–124.
775 Lü, J., Unwin, D.M., Jin, X., Liu, Y., Ji, Q., 2010. Evidence for modular evolution in a long–
776 tailed pterosaur with a pterodactyloid skull. Proc. R. Soc. Lond. B: Biol. Sci. 277, 383–
777 389.
778 Luo, Z., Ji, Q., Yuan, C., 2007. Convergent dental adaptations in pseudo-tribosphenic and
779 tribosphenic mammals. Nature 450, 93–97.
780 Luo, Z., Meng, Q., Ji, Q., Liu, D., Zhang, Y., Neander, A.I., 2015. Evolutionary development
781 in basal mammaliaforms as revealed by a docodontan. Science 347, 760–764.
782 Luo, Z., Yuan, C., Meng, Q., Ji, Q., 2011. A Jurassic eutherian mammal and divergence of
783 marsupials and placentals. Nature 476, 442–445.
784 Lyman, F.E., 1943. Swimming and burrowing activities of mayfly nymphs of the genus
785 *Hexagenia*. Ann. Entomol. Soc. Am. 36, 250–256.
786 Mandeville, C.W., Carey, S., Sigurdsson, H., 1996. Sedimentology of the Krakatau 1883
787 submarine pyroclastic deposits. Bull. Volcanol. 57, 512–529.
788 Manville, V., Németh, K., Kano, K., 2009. Source to sink: a review of three decades of
789 progress in the understanding of volcaniclastic processes, deposits, and hazards. Sediment.

790 Geol. 220, 136–161.
791 Manville, V., White, J.D.L., Riggs, N.R., 2001. Sedimentology and history of Lake Reporoa:
792 an ephemeral supra-ignimbrite lake, Taupo Volcanic Zone, New Zealand. Volcaniclastic
793 Sedimentation in Lacustrine Settings, Int. Ass. Sedimentol. Spec. Publ. 30, 109–140.
794 Martí, J., Groppelli, G., Silveira, A., 2018. Volcanic stratigraphy: a review. J. Volcanol.
795 Geotherm. Res. 357, 68–91.
796 Martínez-Delclòs, X., Martinell, J., 1993. Insect taphonomy experiments. Their application to
797 the Cretaceous outcrops of lithographic limestones from Spain. Kaupia 2, 133–144.
798 Martin, T., Marugán-Lobón, J., Vullo, R., Martín-Abad, H., Luo, Z., Buscalioni, A.D., 2015. A
799 Cretaceous eutriconodont and integument evolution in early mammals. Nature 526, 380–
800 384.
801 Meng, J., Hu, Y., Wang, Y., Wang, X., Li, C., 2006. A Mesozoic gliding mammal from
802 northeastern China. Nature 444, 889–893.
803 Meng, Q., 2003. What drove late Mesozoic extension of the northern China-Mongolia tract?
804 Tectonophysics 369, 155–174.
805 Mulder, T., Alexander, J., 2001. The physical character of subaqueous sedimentary density
806 flows and their deposits. Sedimentology 48, 269–299.
807 Mulder, T., Chapron, E., 2011. Flood deposits in continental and marine environments:
808 character and significance. In: Slatt, R.M., Zavala, C (Eds.), Sediment Transfer from Shelf
809 to Deep Water – Revisiting the Delivery System, AAPG Studies in Geology, 61, pp. 1–30.
810 Na, Y., Manchester, S.R., Sun, C., Zhang, S., 2015. The Middle Jurassic palynology of the
811 Daohugou area, Inner Mongolia, China, and its implications for palaeobiology and

812 palaeogeography. Palynology 39, 270–287.
813 Na, Y., Sun, C., Wang, H., Dilcher, D.L., Li, Y., 2017. A brief introduction to the Middle
814 Jurassic Daohugou Flora from Inner Mongolia. Rev. Palaeobot. Palynol. 247, 53–67.
815 Nelson, C.H., Meyer, A.W., Thor, D., Larsen, M., 1986. Crater Lake, Oregon: A restricted
816 basin with base-of-slope aprons of nonchannelized turbidites. Geology 14, 238–241.
817 Nemec, W., Steel, R., 1988. What is a fan delta and how do we recognize it? In: Nemec, W.,
818 Steel, R. (Eds.), Fan Deltas: sedimentology and tectonic settings. Blackie & Son,
819 Edinburgh, pp. 3–13.
820 Nie, S., Rowley, D., Ziegler, A., 1990. Constraints on the locations of Asian microcontinents
821 in Palaeo-Tethys during the Late Palaeozoic. Geol. Soc. Lond. Mem. 12, 397–409.
822 Niem, A.R., 1977. Mississippian pyroclastic flow and ash-fall deposits in the deep-marine
823 Ouachita flysch basin, Oklahoma and Arkansas. Geol. Soc. Am. Bull. 88, 49–61.
824 Olsen, P.E. 2016. The paradox of “clam shrimp” paleoecology. International Geological
825 Congress, Abstracts, v. 35; 35th International Geological Congress, Cape Town, South
826 Africa, Aug. 27-Sept. 4, 2016.
827 Palmer, B.A., Shawkey, E.P., 1997. Lacustrine sedimentation processes and patterns during
828 effusive and explosive volcanism, Challis volcanic field, Idaho. J. Sediment. Res. 67, 154–
829 167.
830 Palmer, B.A., Shawkey, E.P., 2001. Lacustrine-fluvial transitions in a small intermontane
831 valley, Eocene Challis Volcanic Field, Idaho. In: White, J.D.L., Riggs, N.R. (Eds.),
832 Volcaniclastic Sedimentation in Lacustrine Settings. International Association of
833 Sedimentologists, Special Publication 30, 179–198.

834 Parsons, J.D., Bush, J.W., Syvitski, J.P., 2001. Hyperpycnal plume formation from riverine
835 outflows with small sediment concentrations. Sedimentology, 48, 465–478.
836 Pott, C., Jiang, B., 2017. Plant remains from the Middle–Late Jurassic Daohugou site of the
837 Yanliao Biota in Inner Mongolia, China. Acta Palaeobot. 57, 185–222.
838 Pozzuoli, A., Vila, E., Franco, E., Ruiz-Amil, A., De La Calle, C., 1992. Weathering of biotite
839 to vermiculite in Quaternary lahars from Monti Ernici, central Italy. Clay Minerals 27,
840 175–184.
841 Reineck, H.-E., Singh, I.B., 2012. Depositional sedimentary environments: with reference to
842 terrigenous clastics. Springer Science & Business Media.
843 Ren, D., Gao, K., Guo, Z., Ji, S., Tan, J., Song, Z., 2002. Stratigraphic division of the Jurassic
844 in the Daohugou area, Ningcheng, Inner Mongolia. Geol. Bull. Chin. 21, 584–591.
845 Riggs, N.R., Busby-Spera, C.J., 1990. Evolution of a multi-vent volcanic complex within a
846 subsiding arc graben depression: Mount Wrightson Formation, Arizona. Geol. Soc. Am.
847 Bull. 102, 1114–1135.
848 Schmid, R., 1981. Descriptive nomenclature and classification of pyroclastic deposits and
849 fragments: Recommendations of the IUGS Subcommission on the Systematics of Igneous
850 Rocks. Geology 9, 41–43.
851 Scott, W.E., Hoblitt, R.P., Torres, R.C., Self, S., Martinez, M.M.L., Nillos, T., 1996.
852 Pyroclastic flows of the June 15, 1991, climactic eruption of Mount Pinatubo. Fire and
853 Mud: eruptions and lahars of Mount Pinatubo, Philippines, 545–570.
854 Self, S., 1983. Large-scale phreatomagmatic silicic volcanism: a case study from New
855 Zealand. J. Volcanol. Geotherm. Res. 17, 433–469.

856 Shen, Y., Chen, P., Huang, D., 2003. Age of the fossil conchostracans from Daohugou of
857 Ningcheng, Inner Mongolia. J. Stratigr. 27, 311–313.
858 Sigurdsson, H., Cashdollar, S., Sparks, S.R.J., 1982. The eruption of Vesuvius in A.D. 79:
859 reconstruction from historical and volcanological evidence. Am. J. Archaeol. 86, 39–51.
860 Simon, A., 1999. Channel and drainage-basin response of the Toutle River system in the
861 aftermath of the 1980 eruption of Mount St. Helens, Washington, U.S. Geological Survey
862 Open-File Report, 96-633. 130 pp.
863 Smith, G.A., 1988. Sedimentology of proximal to distal volcaniclastics dispersed across an
864 active foldbelt: Ellensburg Formation (late Miocene), central Washington. Sedimentology
865 35, 953–977.
866 Smith, G.A., 1991. Facies sequences and geometries in continental volcaniclastic sediments.
867 In: Fisher, R.V., Smith, G.A. (Eds.), Sedimentation in Volcanic Settings: Soc. Econ.
868 Paleontol. Mineral. Spec. Publ. 45, 10–25. Tulsa, Ok.
869 Smith, R., 1986. Sedimentation and palaeoenvironments of Late Cretaceous crater‐lake
870 deposits in Bushmanland, South Africa. Sedimentology 33, 369–386.
871 Streck, M.J., Grunder, A.L., 1995. Crystallization and welding variations in a widespread
872 ignimbrite sheet; the Rattlesnake Tuff, eastern Oregon, USA. Bull. Volcanol. 57, 151–169.
873 Sturm, M., 1979. Origin and composition of clastic varves. In: C. Schüchter (ed.), Moraines
874 and Varves. Balkema, Rotterdam, pp. 281–285.
875 Sturm, M., Matter, A., 1978. Turbidites and varves in Lake Brienz (Switzerland): deposition
876 of clastic detritus by density currents. In: Matter, A., Tucker, M.E. (Eds.), Modern and
877 Ancient Lake Sediments. Spec. Publ. Int. Assoc. Sedimentol. 2, 147–168.

878 Sullivan, C., Wang, Y., Hone, D.W., Wang, Y., Xu, X., Zhang, F., 2014. The vertebrates of the
879 Jurassic Daohugou Biota of northeastern China. J. Vertebr. Paleontol. 34, 243–280.
880 Tasch, P., 1969. Branchiopoda, In: Moore R.C., (Ed), Treatise on Invertebrate Paleontology,
881 Part R, Arthropoda 4. 1969, Geol. Soc. Am. and Univ. Kans. Press; Lawrence.
882 Tian, Q., Wang, S., Yang, Z., Jiang, B. in prep. Understanding the rapid burial of articulated
883 carcasses in lacustrine Konservat-Lagerstätten – an experimental approach.
884 Vannier, J., Thiery, A., Racheboeuf, P.R., 2003. Spinicaudatans and ostracods (Crustacea)
885 from the Montceau Lagerstätte (Late Carboniferous, France): morphology and
886 palaeoenvironmental significance. Palaeontology 46, 999–1030.
887 Wang, B., Li, J., Fang, Y., Zhang, H., 2009. Preliminary elemental analysis of fossil insects
888 from the Middle Jurassic of Daohugou, Inner Mongolia and its taphonomic implications.
889 Chinese Sci. Bull. 54, 783–787.
890 Wang, B., Zhang, H., Jarzembowski, E.A., Fang, Y., Zheng, D., 2013. Taphonomic variability
891 of fossil insects: a biostratinomic study of Palaeontinidae and Tettigarctidae (Insecta:
892 Hemiptera) from the Jurassic Daohugou Lagerstätte. Palaios 28, 233–242.
893 Wang, W., Zheng, S., Zhang, L., Pu, R., Zhang, W., Wu, H., Ju, R., Dong, G., Yuan, H., 1989.
894 Mesozoic stratigraphy and palaeontology of western Liaoning (1), Beijing: Geol. Pub.
895 House (in Chinese with English abstract).
896 Wang, X., Wang, Y., Zhang, F., Zhang, J., Zhou, Z., Jin, F., Hu, Y., Gu, G., Zhang, H., 2000.
897 Vertebrate biostratigraphy of the Lower Cretaceous Yixian Formation in Lingyuan, western
898 Liaoning and its neighboring southern Nei Mongol (inner Mongolia), China. Vertebr.
899 Palasiat. 38, 95–101.

900 Wang, X., Zhou, Z., He, H., Jin, F., Wang, Y., Zhang, J., Wang, Y., Xu, X., Zhang, F., 2005.
901 Stratigraphy and age of the Daohugou bed in Ningcheng, Inner Mongolia. Chinese Sci.
902 Bull. 50, 2369–2376.
903 Wang, S., Hethke, M., Wang, B., Tian, Q., Yang, Z., Jiang, B. in prep. High-resolution
904 biostratinomical analysis of Jurassic Yanliao biota from the Daohugou area, NE China.
905 Webb, J., 1979. A reappraisal of the palaeoecology of conchostracans (Crustacea:
906 Branchiopoda). Neues Jahrb. Geol. Paläontol., Abh. 158, 259–275.
907 Whitham, A., 1989. The behaviour of subaerially produced pyroclastic flows in a subaqueous
908 environment: evidence from the Roseau eruption, Dominica, West Indies. Mar. Geol. 86,
909 27–40.
910 Wilson, C., Walker, G.P., 1985. The Taupo eruption, New Zealand I. General aspects. Phil.
911 Trans. R. Soc. Lond. A 314, 199–228.
912 Wohletz, K., 1983. Mechanisms of hydrovolcanic pyroclasts formation: grain size, scanning
913 electron microscopy, and experiments studies. J. Volcanol. Geotherm. Res. 17, 31–64.
914 Xu, H., Liu, Y., Kuang, H., Jiang, X., Peng, N., 2012. U-Pb SHRIMP age for the Tuchengzi
915 Formation, northern China, and its implications for biotic evolution during the Jurassic–
916 Cretaceous transition. Palaeoworld 21, 222–234.
917 Xu, X., You, H., Du, K., Han, F., 2011. An *Archaeopteryx*–like theropod from China and the
918 origin of Avialae. Nature 475, 465–470.
919 Xu, X., Zhang, F., 2005. A new maniraptoran dinosaur from China with long feathers on the
920 metatarsus. Naturwissenschaften 92, 173–177.
921 Xu, X., Zhao, Q., Norell, M., Sullivan, C., Hone, D., Erickson, G., Wang, X., Han, F., Guo, Y.,

2009. A new feathered maniraptoran dinosaur fossil that fills a morphological gap in avian origin. Chinese Sci. Bull. 54, 430–435.

Xu, X., Zheng, X., Sullivan, C., Wang, X., Xing, L., Wang, Y., Zhang, X., O'Connor, J.K., Zhang, F., Pan, Y., 2015. A bizarre Jurassic maniraptoran theropod with preserved evidence of membranous wings. Nature 521, 70–73.

Xu, X., Zhou, Z., Dudley, R., Mackem, S., Chuong, C., Erickson, G.M., Varricchio, D.J., 2014. An integrative approach to understanding bird origins. Science 346, 1253293.

Xu, X., Zhou, Z., Sullivan, C., Wang, Y., Ren, D., 2016. An updated review of the Middle - Late Jurassic Yanliao Biota: chronology, taphonomy, paleontology and paleoecology. Acta Geol. Sin. Engl. 90, 2229–2243.

Yang, W., Li, S., 2008. Geochronology and geochemistry of the Mesozoic volcanic rocks in Western Liaoning: implications for lithospheric thinning of the North China Craton. Lithos 102, 88–117.

Yin, A., Nie, S., 1996. A Phanerozoic palinspastic reconstruction of China and its neighboring regions. World and Regional Geology 1, 442–485.

Wang, Y., 2000. A new salamander (Amphibia: Caudata) from the Early Cretaceous Jehol biota. Vertebr. Palasiat. 2, 002.

Wang, Y., Dong, L., Evans, S.E., 2010. Jurassic–Cretaceous herpetofaunas from the Jehol associated strata in NE China: evolutionary and ecological implications. Bull. Chinese Acad. Sci. 24, 76–79.

Zhang, F., Zhou, Z., Xu, X., Wang, X., Sullivan, C., 2008. A bizarre Jurassic maniraptoran from China with elongate ribbon-like feathers. Nature 455, 1105–1108.

944 Zhang, J., 2002. Discovery of Daohugou Biota (Pre-Jehol Biota) with a discussion on its
945 geological age. J. Stratigr. 26, 173–177.
946 Zhang, Y., Dong, S., Zhao, Y., Zhang, T., 2008. Jurassic tectonics of North China: a synthetic
947 view. Acta Geol. Sin. Engl. 82, 310–326.
948 Zhou, L., Algeo, T.J., Feng, L., Zhu, R., Pan, Y., Gao, S., Zhao, L., Wu, Y., 2016. Relationship
949 of pyroclastic volcanism and lake-water acidification to Jehol Biota mass mortality events
950 (Early Cretaceous, northeastern China). Chem. Geol. 428, 59–76.
951 Zhou, Z., Jin, F., Wang, Y., 2010. Vertebrate assemblages from the Middle-Late Jurassic
952 Yanliao Biota in northeast China. Earth Sci. Frontiers 17: 252–254.
953 Zhou, Z., Zheng, S., Zhang, L., 2007. Morphology and age of *Yimaia* (Ginkgoales) from
954 Daohugou Village, Ningcheng, Inner Mongolia, China. Cretaceous Res. 28, 348–362.
955 Ziegler, A.M., Rees, P.M., Rowley, D.B., Bekker, A., Qing, L., Hulver, M.L., 1996. Mesozoic
956 assembly of Asia: constraints from fossil floras, tectonics, and paleomagnetism. In: Yin, A.,
957 Harrison, T.M. (Eds.), Tectonic evolution of Asia. Cambridge Univ. Press, Cambridge, pp.
958 371–400.

Appendix 1. Supplementary methods

1. X-ray diffraction analysis

Two specimens of insect-bearing laminated mudstone were pulverized without cross contamination before XRD analysis. The prepared samples were then analyzed for mineralogy by XRD using Rigaku, Ultima IV with D/teX Ultra, at the Institute of Soil Science, Chinese Academy of Science.

2. Plan-view orientation measurement

Plan-view orientations of the aquatic insects *Fuyous gregarious*, *Shantous lacustris*, and *Daohugocorixa vulcanica* were obtained from nine horizons (A1, B1, B2, C1, E2, F1, I1, I3, I4, Fig. 2A) by scoring the orientation of each individual based on a twelve-fold segmentation of the full circular arc of 360°. Two individuals whose heads point in opposite directions are treated as showing the same orientation. Hence, the segments 7–12 were mirrored, and only six directions (0–180°) remained to test for preferred orientations using Rayleigh's test and the Chi-square test (Hethke et al., submitted). Rayleigh's test is based on data drawn from a population with a von Mises distribution (Davis, 1986). Rayleigh's test has the following null and alternative hypotheses:

H_0: the orientations of the aquatic insects are uniformly distributed

H_1: there is a single preferred orientation

Similarly, the null and alternative hypotheses of Chi-square test are:

H_0: the orientations of the aquatic insects are uniformly distributed

H_1: the orientations of the aquatic insects are not uniformly distributed

These two tests are used together to test for preferred orientations using the scheme of Hammer and Harper (2006).

References

Davis, J., 1986, Statistics and Data Analysis in Geology, John Wiley & Sons Canada, Ltd.

Hammer, Ø., Harper, D., 2006 Paleontological data analysis. – Blackwell Publishing.

Hethke, M., Fürsich, F.T., Jiang, B., Wang, B., Chellouche, P., Weeks, S.C. submitted. Ecological stasis in Spinicaudata (Crustacea: Branchiopoda)? – Early Cretaceous clam shrimp of the Yixian Formation of NE China occupied a broader realized ecological niche than extant members of the group. Palaeontology.

Appendix 2. Supplementary results

1. X-ray diffraction (XRD) analysis

	Montmorillonite	Vermiculite	Illite	Aluminite	Quartz	Feldspar	Dolomite
Sample 1	24%	26%	22%	0%	14%	12%	2%
Sample 2	19%	19%	11%	14%	17%	19%	1%
Mean	21.5%	22.5%	16.5%	7%	15.5%	15.5%	1.5%

Table 1 XRD analysis of the fossil-bearing mudstone from Unit 3.

2. Plan-view orientation

Horizons	n	Mean	R	P (Rand)	Chi^2	P (Rand)
A1	16	83.05	0.23	0.45	6.5	0.26
B1	16	96.95	0.23	0.45	5	0.42
B2	77	27.64	0.14	0.24	39.96	1.52E-07
C1	103	68.74	0.11	0.28	33.49	3.01E-06
E2	13	45	0.27	0.41	8.69	0.12
F1	27	83.05	0.13	0.62	16.33	0.0060
I1	17	60	0.35	0.12	6.65	0.25
I3	110	86.39	0.19	0.02	26.58	6.88E-05
I4	24	80.45	0.11	0.75	10	0.075

Table 2 Test results (Rayleigh and Chi-square) based on directional measurements of aquatic insects in nine horizons (locations shown in Fig. 2A).

Based on the results of the Chi-square test, the aquatic insects in horizons B2, C1, F1 and I3 exhibit preferred orientations. The null hypothesis of random orientation can be rejected at a significance level of 1%. Among these four horizons, Rayleigh's test further indicates a single preferred orientation in I3 at 5% significance level, while the null hypothesis could not be rejected for B2, C1, and F1, implying two or more preferred orientations in the respective horizons (Appendix 2, Table 2).